frontiers | Frontiers in Nanotechnology

TYPE Original Research
PUBLISHED 12 April 2023
DOI 10.3389/fnano.2023.1135835

OPEN ACCESS

EDITED BY
Ricardo Paupitz Barbosa Dos Santos,
São Paulo State University, Brazil

REVIEWED BY
Yingchao Yang,
University of Maine, United States
Alex Otávio Sanches,
São Paulo State University, Brazil

*CORRESPONDENCE
Stanislav A. Moshkalev,
stanisla@unicamp.br

SPECIALTY SECTION
This article was submitted to Nanomaterials, a section of the journal Frontiers in Nanotechnology

RECEIVED 01 January 2023
ACCEPTED 27 March 2023
PUBLISHED 12 April 2023

CITATION
Nista SVG, Alaferdov AV, Isayama YH, Mei LHI and Moshkalev SA (2023), Flexible highly conductive films based on expanded graphite /polymer nanocomposites. *Front. Nanotechnol.* 5:1135835. doi: 10.3389/fnano.2023.1135835

Flexible highly conductive films based on expanded graphite /polymer nanocomposites

Silvia V. G. Nista[1], Andrei V. Alaferdov[2], Yuri H. Isayama[1], Lucia H. I. Mei[3] and Stanislav A. Moshkalev[1]*

[1]Center for Semiconductor Components and Nanotechnology (CCSNano), UNICAMP, Campinas, Brazil, [2]Eldorado Research Institute, Campinas, Brazil, [3]Department of Materials and Bioprocess Engineering (DEMBio), Faculty of Chemical Engineering, UNICAMP, Campinas, Brazil

Highly electrically and thermally conducting films of expanded graphite/polymer nanocomposites were fabricated using an approach based on solution mixing methods. The use of Hydroxyethylcellulose and benzylic alcohol based solutions provides efficient dispersion and better exfoliation of multilayer graphene (nanographite) flakes that are further aligned in extended 2D layers forming continuous conductive pathways during lamination (hot calendering) process. Very high electrical conductivity (190 S/cm) was obtained for fabricated layered films. In contrast, for films produced by a conventional mixing and deposition method with acrylic copolymer and the same nanographitic material, with flakes randomly distributed within the composite, much lower conductivities (2.4 S/cm) were obtained.

KEYWORDS

nanographite, expanded graphite, composite, hydroxyethylcellulose, electrical and thermal conductivity, graphene

1 Introduction

The search for novel composite materials to fabricate flexible conductive films was carried out by the scientific and technological community in recent years. Flexible graphene and nanographite based films have numerous applications due to their high electrical and thermal conductivity, resilience, fluid impermeability, chemical resistance, resistance to high temperatures and low thermal expansion. Some of these applications are fuel cell components (Rashid et al., 2021), electrochemical electrodes (Hareesha and Manjunatha, 2020), solar cell (Cho et al., 2020), thermal interface materials (Hu and Chung, 2011; Fu et al., 2019), miniaturized heaters, sensors, absorbers or heat sinks, among others (Chung, 2016).

Due to the presence of sp^2 hybridized carbon atoms, monolayer graphene is highly electrically and thermally conductive. In particular, thermal and electrical conductivities of a monolayer graphene are 3000 W/mK and 6000 S/cm, respectively (Zotti et al., 2022).

The use of high-quality low-dimensional carbon nanostructures as single- or multiwall nanotubes or monolayer graphene in nanocomposites has been limited by challenges in processing and dispersion, but the biggest obstacle to their extensive use was the relatively high price (up to hundreds of US$/kg, until recently), making their applications in composites for large-scale production unfeasible. On the other hand, multilayer 2 D graphitic materials like nanoplatelets of multilayer graphene (MLG), graphite nanoplatelets or expanded graphite (EG) obtained from natural graphite with much lower cost, being as low as US$ 2/kg (Frac et al., 2020), have electrical and thermal properties comparable with those for monolayer graphene thus making them promising

for such applications. Multilayer graphene consists of stacked graphene layers joined by van der Waals forces (Li and Zhong, 2011; Chung, 2016).

Expanded graphite currently is produced in industrial scale, by submitting flakes of natural graphite to treatment with sulfuric acid readily intercalating between the graphitic layers, followed by a thermal shock (Vieira et al., 2006). A great expansion of graphite flakes occurs in the cross-plane direction, forming vermicular structures with low mass density, excellent resistance to high temperatures, and a good affinity for organic compounds and polymers (Sengupta et al., 2011). Thus, EG and its derivatives (that are in fact partially oxidized graphite nanoplatelets) are promising low-cost materials for preparing nanocomposites, due to their multifunctionality well suited for practical applications.

Purely graphitic flexible highly conducting films can be also produced, and normally the fabrication process consists of compression of the material under a predetermined load, in the absence of a binder (Chung, 2016; Fu et al., 2008). If the compaction pressure is high enough, the process results in a reasonably strong sheet, due to the cellular structure and the consequent mechanical interlocking between the MLG flakes. These sheets are known as flexible graphite films, commercially available, being used nowadays mainly as a sealing material for fluids (Chung, 2016). The electrical and thermal conductivities of the resultant exfoliated graphene paper are as high as 2200 S/cm and 1500 W/m.K (C. Teng et al., 2017). However, due to high complexity of working with particulate materials, and the need for specific equipment to compress this kind of material, large-scale production becomes a serious issue due to occupational risks with suspended particulate materials (Kondo et al., 1981).

The preparation of graphite nanocomposites with polymers as binders is a promising alternative. The advantages of these nanocomposites in comparison with pure graphitic materials, are in ease of handling and preparation, higher mechanical resistance, better flexibility, durability, and relatively low cost of production. Several works can be cited regarding the preparation of conductive materials, using carbon in its various allotropic and granular forms, mixed with polymers such as PVC (Mindivan and Göktaş, 2020), PTFE (Aturaliya et al., 2020), polyethylene (Li L. et al., 2020), polystyrene (Das and Prusty, 2013), cellulose acetate (Han et al., 2020), epoxy adhesive (Li L. et al., 2020), silicone rubber (Kurian et al., 2020), among others. However, it should be noted that carbon/polymer composites have considerably reduced electrical/thermal conductivities as organic polymers are electrically insulating.

The challenge of making conductive nanocomposites involves the choice of a suitable mixing method to achieve a satisfactory dispersion between graphitic material and polymer (Li and Zhong, 2011). In the preparation of nanographite based nanocomposites using the solution mixing methods (López-Machado et al., 2004; Ding et al., 2012; Zanrosso et al., 2020), the polymer is dissolved in a solvent and the graphite is dispersed in the resulting solution. After mixing, the solvent is removed by curing, and the polymeric material is molded, to form the composite. This technique results in electrically conductive composites with a low percolation threshold.

There are two main approaches to form a conductive network within a hosting polymer matrix: 1) A conventional method, with filler particles uniformly distributed within the matrix (random distribution conductive network), and 2) a segregated conductive network, with fillers selectively distributed at the interfaces between polymer granules thus generating more efficient conductive pathways, due to formation of layered structures (highly conducting layers within the hosting matrix) (Li et al., 2013; Alaferdov et al., 2022). Using the conventional approach, higher percolation thresholds and relatively low electrical conductivities using graphene and its derivatives, up to 1 S/cm, were reported (Zotti et al., 2022). In contrast, the segregation based method using a hot calendering process, that results in high degree of alignment for 2 D graphitic fillers, has shown several important advantages including lower percolation thresholds and enhanced conductivities due to higher local concentration of filler elements providing more efficient conductive pathways. Electrical conductivity up to 40 S/cm was obtained for composites consisting of UHMWPE polymer and graphite nanoplatelets (Alaferdov et al., 2022). Another approach to obtain highly aligned layered graphene films in a polymer matrix has been recently demonstrated by Zhuang et al. (2021), where high orientation and in-plane alignment of graphene flakes were achieved. For this, efficient dispersants like aqueous solutions of naphthalene sulfonate were used, followed by a layer-by-layer scraping deposition process with multiple deposition/solvent evaporation steps. Due to sequential solvent evaporations steps, films with dense graphene containing layers (up to 66% w/w) were formed. In this way, it was possible to obtain free standing graphene based films with extremely high in-plane electrical and thermal conductivities (1.25×10^3 S/cm and 300 W/m.K), however this method seems to be difficult to scale up. Another examples of layered composite films fabricated using HEC, HPMC, and PVA polymer aqueous solutions and reduced graphene oxide (rGO) were reported by Wang et al. (2018), however probably due to low degree of post-deposition GO reduction, conductivities below 1 S/cm were obtained.

The material developed in this work consists of a new highly conductive graphite nanoplatelets/polymer nanocomposite for fabrication of flexible films, based on low-cost expanded graphite, with high electrical and thermal conductivity, low cost, and ease of processing. The approach used in this work is the preparation of nanocomposites by the solution mixing methods with Hydroxyethylcellulose and benzylic alcohol based solutions that provide efficient dispersion and better exfoliation of graphite nanoplatelets that can be further aligned in extended 2D layers forming electron conductive pathways during lamination (hot calendering) process.

2 Experimental

The nanographite powder produced from expanded graphite (Micrograph HC30) was supplied by Nacional de Grafite Ltda, Brazil. Hydroxyethylcellulose or HEC (QP100) was supplied by Dow Chemical. Benzylic alcohol from Merck and distillate water were used to prepare all the solutions. For comparison, some samples were prepared using only water as a solvent. For comparative tests, acrylic copolymer solutions in water emulsion (solid part of 52%, viscosity 850cP at 25°C), Wana Quimica (Brazil) were also used.

The HEC based nanocomposites were prepared by mixing nanographite powder with polymers and solvents (benzylic alcohol and water), with high degree of graphite/polymer dilution. The mixtures were stirred continuously for 10 min at a room

temperature to prepare the sample paste. The paste was spread on a paper substrate and calendered. The sample was dried for 4 h at 90°C and then calendered again at the temperature of 120°C for better alignment and film compaction until approximately 0.2 mm. Volume fractions of graphite in the films were varied in a wide range, from 0.6% to 65% v/v. An example of a mixture formulation (in % w/w), where the percolation threshold was detected: GE/HEC/benzylic alcohol/water = 0.3/1.1/42.5/55.7. Assuming full solvent evaporation during the film fabrication, the corresponding graphite/polymer volume fraction in the film is ~0.63% v/v.

The nanographite powder samples were characterized using scanning electron microscopy—SEM (FIB/SEM dual-beam system, Nova 200 Nanolab, FEI) equipped with energy-dispersive X-ray spectroscopy—EDS detector (X-Max, Oxford Instruments), and high resolution transmission electron microscopy—TEM (JEOL JEM-2100, JEOL Ltd). The crystalline quality of samples was analyzed by confocal micro-Raman spectroscopy (NT-MDT NTEGRA Spectra, with a 473 nm laser). The crystallographic structure was determined by powder X-ray diffraction—XRD method (Bruker: D2 PHASER equipped with Cu Kα radiation source, λ = 0.15418 nm and high resolution LYNXEYE XE-T detector, without use of additional filters or monochromator). The X-ray photoelectron spectroscopy—XPS was employed for detailed analysis of chemical composition, using a SPECS system (SPECS GmbH, Germany) equipped with XR 50- X-ray source with Al Kα radiation (hν 1486.6 eV) and Phoibos 100 hemispherical energy analyzer with MCD-9 detector.

The crystallite size L_c was determined from (002) XRD peak using the Scherrer equation: $\boldsymbol{L_c} = \frac{\mathbf{0.89 \cdot \lambda}}{\boldsymbol{B \cdot cos\,\theta}}$, where λ is wavelength of X-ray source, B is full width half maximum of (002) XRD peak component (Bernal component) and θ is the Bragg angle. The deconvolution process of C_{1s} peak was performed in program Peakfit version 4, AISN Software Inc., using the Voight shape of fitting curves. The in-plane crystallite size L_a was calculated using the equation (Ganguly et al., 2011): $L_a\,(nm) = 2.4 \cdot 10^{-10} \cdot \lambda_L^4 \cdot (\frac{I_D}{I_G})^{-1}$, where I_D and I_G are integral intensities of D and G lines of Raman spectra, respectively, and λ_L is the laser wavelength (in nm).

The nanographite based flexible conductive films were investigated by SEM in Leica equipment (Model LEO 440i). Before the SEM test, nanostructured composite films were dried under vacuum 0.1 mbar and coated with gold to determine the morphology. The electrical resistivity measurements were conducted for the in-plane direction using the four-probe method, employing the Agilent® B2912A Series Low Noise Power Source. Cross-plane thermal conductivity tests were performed using the method described by Danes et al., 2003.

3 Results and discussion

The nanographite powder used here was Micrograph HC30, derived from the expanded graphite by mechanical processing, supplied by National de Grafite, Brazil. Exfoliation of natural graphite with intercalating acid is currently the most productive and commercially favorable approach. Graphite nanoplatelets have irregular shapes, lateral sizes that vary from few to few tens of microns (typically, up to 30 μm) and thickness from few to few tens of nanometers. In the exfoliation process, partial oxidation of EG is inevitable, leading to residues of graphite oxide and many hydroxyls, epoxide, and carbonyl groups. These functional groups can form a strong interaction with the polymeric matrix containing polar groups; on the other hand, they provide reactive sites for various types of surface functionalization (Li and Zhong, 2011).

A high degree of crystallinity of the material was proved by XRD and Raman spectroscopy (Figure 1). Deconvolution of the (002) XRD peak results in two components: the main peak located at 26.64° corresponding to Bernal-stacked (ABAB) graphite (Bernal, 1924; Lespade et al., 1984; Alaferdov et al., 2018; Alaferdov et al., 2020) and a secondary peak at 26.43° associated with rhombohedral phase (ABCABC) of graphite (Lespade et al., 1984) (Figure 1A). The deconvolution results indicate that sample is composed predominantly (89.3%) of Bernal-stacked graphite with the interlayer distance near 3.35 Å. Analysis of XRD and Raman spectra also indicates that samples have a polycrystalline structure with crystallite sizes ($L_c \times L_a$) about 25 nm × 65 nm. Notable that the relatively narrow G-band (FWHM about 24 cm^{-1}) and the shape of 2D band typical for nanographite also point out to high crystalline structure quality of samples (Figure 1B) [Pimenta et al., 2007; Alaferdov et al., 2018).

Along with this, EDS analysis carried out on a HC-30 powder indicates the presence of 5.1 ± 0.2 at. % of oxygen atoms (Figure 2A). Further, XPS investigation established that these oxygen atoms form predominantly C-OH configurations (see the area of a C-OH component in Figure 2B) on the surface layers of graphite nanoplatelets.

The deconvolution procedure of the C_{1s} peak (Figure 2B) results in six components. Using data presented in literature (Vanquickenborne et al., 1974; Biniak et al., 1997; Kundu et al., 2008; Cançado et al., 2011; Ren et al., 2011; Perrozzi et al., 2013; Yamada et al., 2013; Reiche et al., 2014), these components of the peak can be assigned to the following carbon atoms configurations: Peaks at 1) 284.4 eV (C = C, sp^2 carbon) and 2) 284.9 eV (C-C, sp^3-carbon) associated with non-oxygenated carbon bonded atoms, 3) at 285.5 eV with C-atom bonded to O in C-OH functional group (hydroxyl group) or C-H bonded atoms in aliphatic configuration, 4) at 286.5 eV with C in an epoxy group (C-O-C), 5) at 287.5 eV with carbon double bonded to oxygen atoms (C = O)—carbonyl group in esters and 6) at 289.1 eV with carbon triple bonded to oxygen atoms (O-C = O) in carboxylic anhydride or carboxylate. Considering together the XRD, EDS and XPS data, one can conclude that surface layers of nanographite are highly functionalized by mostly hydroxyl groups while the main part of material maintains a high degree of crystallinity.

Analysis performed using TEM showed a very non-uniform internal structure of EG samples. In Figure 3, TEM images of a typical nanographite flake deposited from a suspension over an amorphous carbon TEM grid are shown. In the top-view images with higher resolution (Figures 3B, C), it is possible to observe that the flake is composed by many thinner and mostly flat nanoplatelets with lateral sizes down to sub-micron. Cross-sections of some platelets are show in Figures 3D, E, with their thicknesses being as small as 5–10 nm (15–30 graphene layers). Analysis of the images indicates that exfoliation of graphite can produce very thin platelets that further can be partially re-agglomerated during preparation of suspensions and deposition of samples for tests.

It was possible to obtain stable films supported on standard A4 paper sheets (150 g/m^2) for HEC based films, with thicknesses near 0.18 ± 0.03 mm and specific mass in the range from 0.5 to

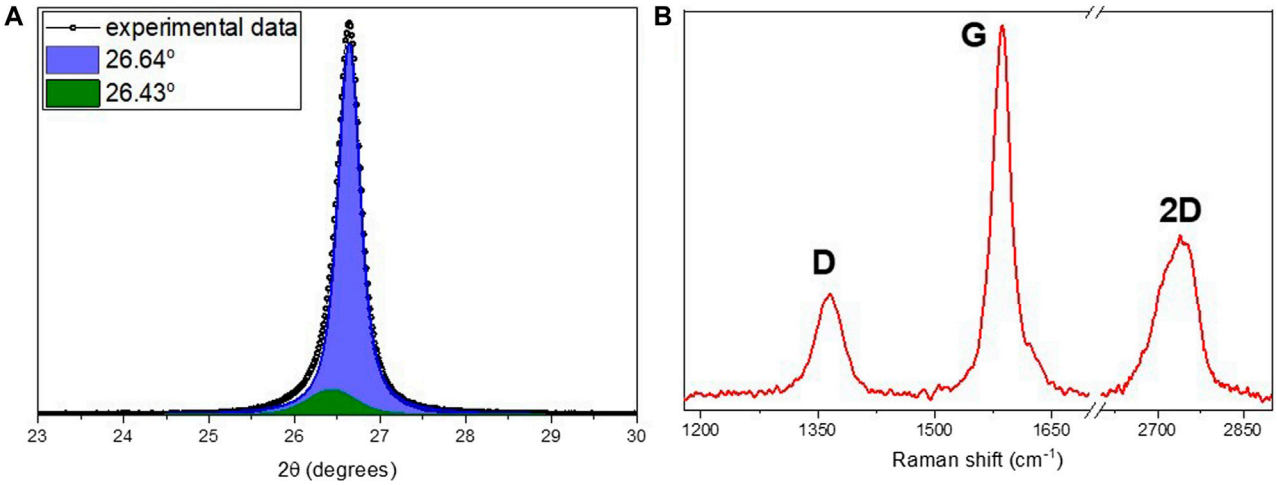

FIGURE 1
(A) Results of deconvolution of (002) XRD peak obtained for HC-30 powder. **(B)** The typical Raman spectra for HC-30 powder, with D, G, and 2D bands shown.

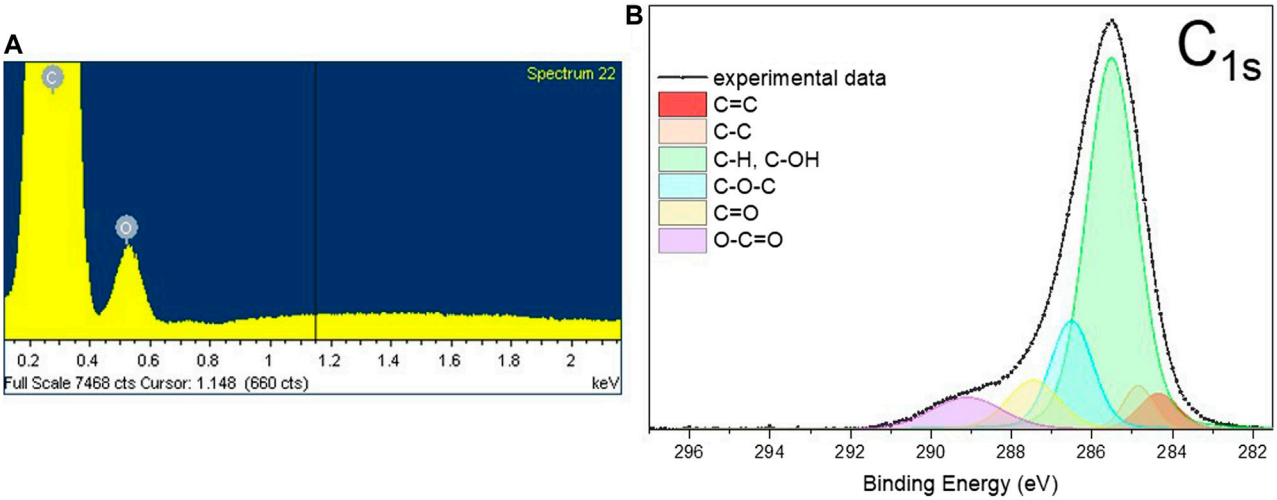

FIGURE 2
The typical EDS spectra **(A)** and the results of deconvolution of C_{1s} XPS peak **(B)** obtained from HC-30 powder sample.

1.2 g/cm^3. An example of a conducting film can be seen in Figure 4. The best results in terms of electrical conductivity, above 1.2 × 10^2 S/cm were obtained for samples with both benzylic alcohol and water used as solvents. For samples with water as a solvent, conductivities below 1.0x10^2 S/cm were measured, still being among the best results reported in literature. An example of a conducting film can be seen in Figure 4. Mechanical characteristics such as Young`s module and tensile strength were measured following the ASTM D882-02 Standard. The calculated mechanical parameters, Young`s module and tensile strength, are presented in Table 1. In comparison, results of mechanical characterization of supporting paper sheets is also presented. It is possible to note that mechanical properties of HEC based films are quite close to those of supporting paper sheets. In other words, integrity of composite films is mostly determined by the supporting paper sheet.

In Figure 5, SEM top-view images of HEC based films are presented. The images clearly show alignment between densely packed irregular-shape graphite flakes and their orientation along the film surface. The best conductivity results, obtained with the addition of benzyl alcohol, can be explained by the fact that benzyl alcohol oxidizes in the presence of graphite providing carbon products with higher conductivities, as reported by Dreyer et al. (2011), Sundar and Subramanian, 2013, Saglam et al. (2016) and Vithalani et al. (2018). As previously mentioned, the oxidation of EG forms inevitable residues of graphite oxide and many hydroxyls, epoxide, and carbonyl groups (Li

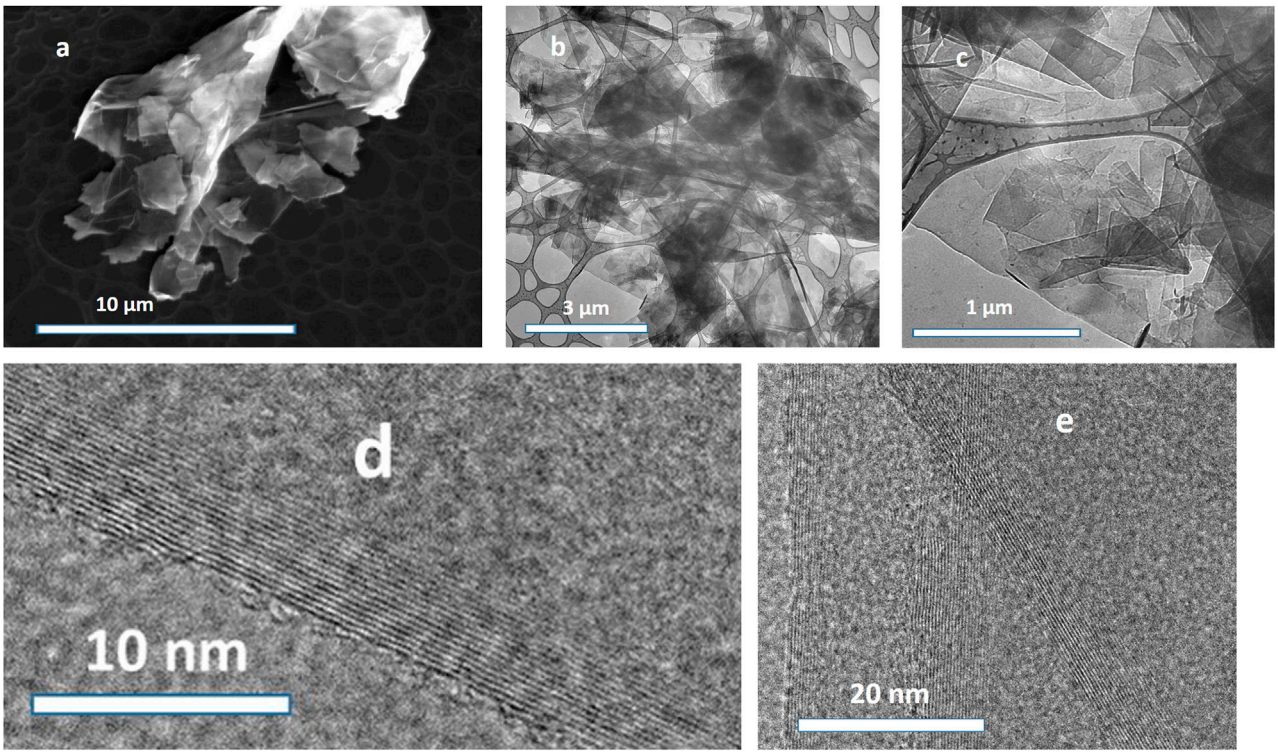

FIGURE 3
TEM images of a nanographite: **(A–C)** top views, **(D, E)** cross-sections.

FIGURE 4
Conductive flexible film, A4 size, HEC sample.

TABLE 1 Data on mechanical characterization of films, tensile tests.

Sample	Young Modulus (MPa)	Tensile Strength (MPa)
HEC/paper	2399	14.1
Paper	3788	17.9
Acrylic	2004	8.8

and Zhong, 2011). Dreyer et al. (2011) showed that graphite oxide (GO) can be used to catalyze the oxidation of a variety of benzyl and aliphatic alcohols, effectively reducing GO and graphene oxide, in materials with higher conductivities. This redox reaction occurs under mild heating conditions at 100°C in the air atmosphere, leading to 350% increase of the C:O ratio in the product, with the conductivity of the material increasing from 2.10^{-5} S/m to 15 S/m (Li et al., 2010). The increase in

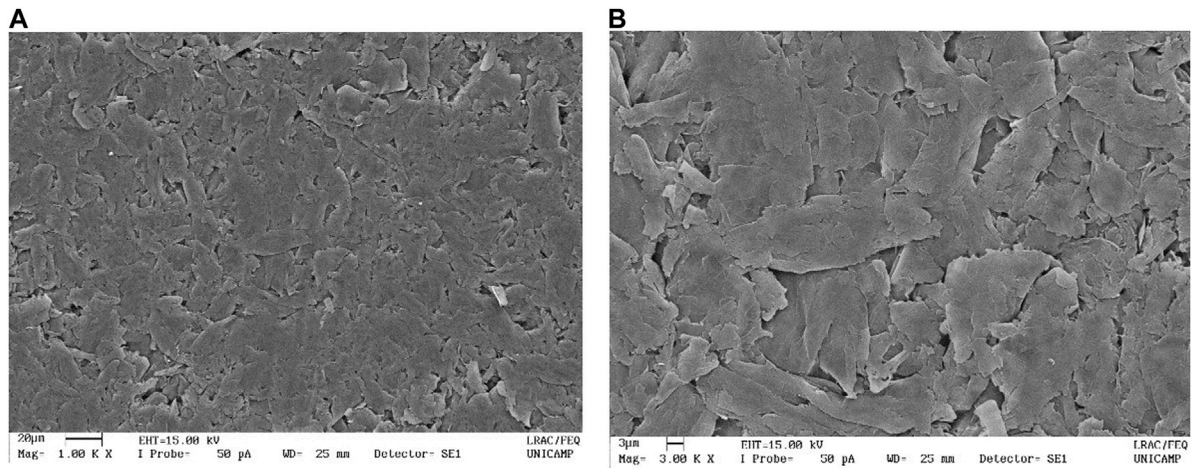

FIGURE 5
SEM images of HEC sample: **(A, B)** top view, scale bars 20 and 3 µm, respectively.

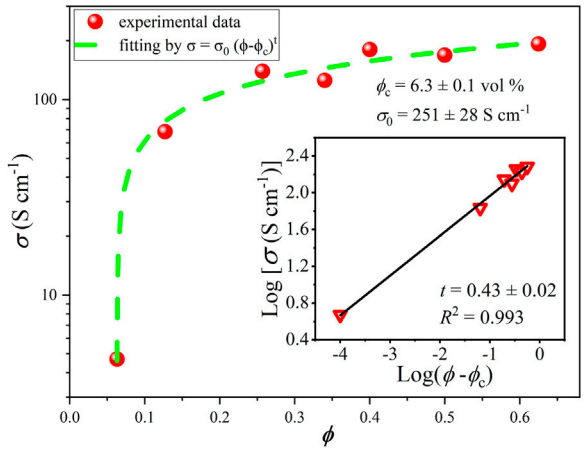

FIGURE 6
Electrical conductivity *vs.* nanographite volume fraction for HEC samples.

the volume of benzyl alcohol and the time of contact between the two reagents improves the efficiency of the reaction. Several mechanisms for this reaction have been proposed in the literature, however, Luo et al. (2014) proposed probably the most plausible mechanism, where benzyl alcohol is oxidized to benzaldehyde and graphite/graphene oxide is reduced producing graphite of greater purity.

The XPS analysis (Figure 2) shows functional groups characteristic of GO, which are reduced by benzyl alcohol, such as ether, ester, aldehydes, and ketones groups. Thus, for the films produced in this work, it is believed that the same reaction may be taking place in interaction between EG with benzyl alcohol before mixing with polymer until the final film is produced. After spreading the paste, drying occurs at 90°C for 3 h where the oxidation reaction probably results in a higher degree of conversion. After drying, the material it is still laminated using calendering at 120°C, continuing the EG reduction process.

Using the formulation with the best resistivity (HA), the graphite fraction in the composite was further varied in a wide range, and the variation of conductivity with graphite percentage is shown in Figure 6. It is possible to see that the conductivity grows fast above the percolation threshold near 0.7% v/v, with much slower rise after 3% v/v. Fitting of the curve using Eq. 1:

$$\sigma = \sigma_0 (\phi - \phi_c)^t \quad (1)$$

known from the classical percolation theory (Shi et al., 2018; Alaferdov et al., 2022), where σ_0 and ϕ are the intrinsic conductivity and volume fraction of the filler, respectively, ϕ_c is the percolation threshold and t is the critical exponent, describing dimensionality of the conductive network: values $t \leq 1.3$ are typical usually for 2D systems, while higher t values are usually associated with 3D filler networks. The fitting gives relatively low value of $t = 0.42$ for HEC based composite indicating 2D character of conducting network and the threshold ϕ_c = 6.3%. The intrinsic conductivity obtained from the fitting, $\sigma_0 = 251 \pm 28$ S/cm, is an order of magnitude smaller than the typical conductivity of films prepared by high pressure compaction of EG flakes, $\sim 2.3 \times 10^3$ S/cm (Chung, 2016).

For comparison, similar curves were obtained here using conventional mixing procedures and doctor blade deposition (without or with weak alignment of platelets) for composites fabricated with the same nanographitic material (HC-30) and acrylic copolymer as a binder with *in situ* polymerization. In this case, due to better mechanical properties, it was possible to obtain stable free standing films with thicknesses in the range from 0.2 to 0.5 mm and measured values of Young`s module and tensile strength are 2004, 8.8 MPa, respectively. In striking contrast to the HEC based films, much higher threshold (23% v/v) and much lower conductivities (2.4 S/cm) were measured (Figure 7). After fast initial rise, the σ(ϕ) curve tends to saturate and then drop for nanographite volume fractions exceeding 0.5. For these samples, cross-plane thermal conductivities were also measured (Figure 8). Relatively high values, up to k = 3.2 W/m.K were obtained, with slow but steady growth until the highest nanographite fractions (90%).

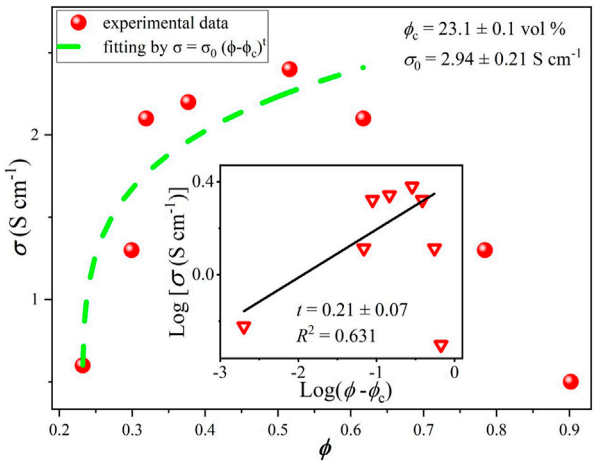

FIGURE 7
Electrical conductivity *vs.* nanographite volume fraction for samples produced with acrylic polymer as a matrix.

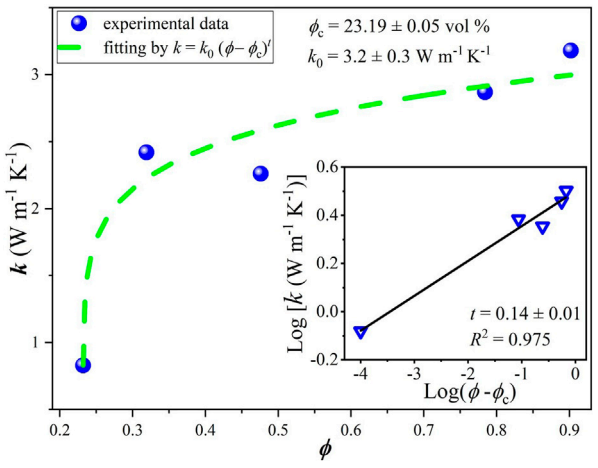

FIGURE 8
Thermal conductivity *vs.* nanographite volume fraction for samples produced with acrylic polymer as a matrix.

The dramatic difference in threshold values and maximum obtained conductivities between HEC and acrylic based samples (Figures 6, 7, respectively) can be probably explained by different distribution of graphite nanoplatelets within the composite, besides the effects associated with the benzyl alcohol solvent (see above). We suggest that HEC based solutions (the first case) provide more efficient dispersion and better exfoliation of graphite nanoplatelets that can be further aligned in extended 2D layers forming electron conductive pathways during lamination (hot calendering) process. In the second case, higher solvent viscosity does not allow efficient dispersion of platelets, and lamination also was not applied, resulting in random distribution and lack of preferential orientation of platelets in the composite and much higher percolation threshold. Increasing of the graphite fraction in this situation can even lead to decreasing degree of platelets orientation and thus, drop in the in-plane electrical conductivity. It is also clear that, in contrast, for cross-plane thermal conductivity (by phonons) higher density of nanographite flakes can favor enhanced percolation probability and enhanced heat transfer.

The obtained results and comparison with other works from literature, for different matrixes and conductive fillers, are summarized in Table 2. Data presented in Table 2 demonstrate very large variety of fitting parameters t, threshold ϕ_c, and maximum achieved conductivities, however some general trends can be confirmed, valid for electrical conductivity: 1) higher t values (indicating 3 D dimensionality of conductive networks) are usually associated with high aspect ratios (length/thickness) fillers like nanowires and nanotubes that readily form 3D networks; 2) composites with higher threshold values are usually less conductive.

Classical percolation theory predicts that the critical exponent has universal values of 1.33 and 2 for two and three dimensional systems, respectively, however a wide variation of this parameter was observed in experiments, for example, in carbon nanotubes based composites the obtained t values were found to range from 0.7 to 3.1 (Forero-Sandoval et al., 2022). This is related to the complexity of transport processes in real systems, characterized by large variations of contact resistances, conductivity and aspect ratios of fillers, tunneling phenomena, effects associated with possible impurities and pores etc. The percolation theory perfectly explains exponential rise of conductivity just above the threshold, however it has limited practical applicability for higher filler contents. In a particular case shown in Figure 7, slower rise or even drop of electrical conductivity with filler volume density approaching 50% may be attributed to poor alignment of flakes during mixing and deposition processes due to “crowding effect”. To lesser extent, this is also valid for thermal conductivity data (Figure 8), where cross-plane conductivity still continues to rise slowly till the highest filler content.

It should be noted that underlying mechanisms responsible for electrical and thermal conductance (electron and phonon transport in multicomponent media) are much different, however for interpretation of thermal related experimental data the same approach based on percolation theory is frequently used and may be really useful at least for data comparisons. In contrast to electrical percolation, even the existence of thermal percolation is still under discussion (Shi et al., 2018). In part this is due to lack of clear observations of a percolation threshold and exponential dependence above the threshold in composites, as polymers are usually good electrical isolators but can conduct heat although typical values of their thermal conductivities are usually quite low, in the order of 0.1 W/m.K.

Interesting to observe that in spite of huge difference in the maximum achieved in-plane electrical conductivity for two composites developed here (190 S/cm and 2.4 S/cm for HEC and acrylic based, respectively), the acrylic based composite is better thermal conductor, as seen in Table 2 (3.2 W/m.K *vs.* 1.65 W/m.K for acrylic and HEC). Better conditions for cross-plane conductivity in acrylic based composite can be explained by random orientation of the nanoplatelets (without preferential alignment in the lateral direction) and thus more possibilities for percolation in the vertical direction.

4 Conclusion

The composite material developed in this work was used for fabrication of highly compacted flexible films, based on low-cost

TABLE 2 Data on electrical and thermal conductivities and their fitting using Eq. 1. PMMA—Poly (methyl methacrylate), UHMWPE—Ultra high molecular weight polyethylene, SWNT—Single wall carbon nanotubes. PLA—Poly lactic acid.

Matrix	Filler	Filler aspect ratio	Critical exponent, t	Percolation threshold, ϕ_c	Maximum value	Ref.
HEC	EG	Medium	0.42	6.3%	190 S/cm	This work
Acrylic	EG	Medium	0.21	23%	2.4 S/cm	This work
UHMWPE	Graphite nanobelts	High	1.39	0.42%	40 S/cm	Alaferdov et al. (2022)
Zinc phosphate glass	Micrographite	Low	1.63	3.48%	3.02×10^{-2} S/cm	Radouane et al. (2020)
PMMA	SWNT	High	2.25	0.3%	1.2×10^{-2} S/cm	Bonnet et al. (2007)
PLA	Graphene nanoplatelets	High	1.32	4.5%	10^{-3} S/cm	Sabzi et al. (2013)
Poly (vinylidene fluoride), PVDF	rGO	Medium	1.1	0.1%	3×10^{-4} S/cm	Li M. et al. (2020)
PVDF	Ag nanowires	High	2.0	2.25%	$1.02x10^{4}$ S/cm	Shi et al. (2018)
HEC*	EG	Medium	-	-	1.65/m.K	This work
Acrylic	EG	Medium	0.14	23%	3.2/m.K	This work
PVDF	Ag nanowires	High	1.93	2.9%	8.43/mK	Shi et al. (2018)

*Measured for free standing samples, 6% v/v.

expanded graphite, with high electrical and thermal conductivity, and ease of processing. The approach used in this work is based on preparation of nanocomposites by the solution mixing methods with Hydroxyethylcellulose (HEC) and benzylic alcohol based solutions that provide efficient dispersion and better exfoliation of MLG flakes that can be further aligned in extended 2D layers forming electron conductive pathways oriented along the film direction during lamination (hot calendering) process. Very high electrical conductivity (190 S/cm) was obtained for fabricated layered films, being one of the best reported in literature. In contrast, for films produced by a conventional mixing and deposition method (characterized by random distribution of fillers within the composite) using acrylic copolymer and the same nanographitic material, almost two orders of magnitude lower conductivities (2.4 S/cm) were obtained. Interestingly, higher cross-plane thermal conductivities were obtained for acrylic copolymer based films, up to 3.2 W/m.K, compared with 1.65 W/m.K for HEC based films.

Data availability statement

The raw data supporting the conclusion of this article will be made available by the authors, without undue reservation.

Author contributions

SN: Material fabrication, measurements, data analysis and writing, AA: TEM, EDS, XPS, and XRD measurements, data analysis, editing; YI: Thermal measurements; LM: Material fabrication, writing; SM: Funding, writing and data analysis. All authors contributed to the article and approved the submitted version.

Funding

The work was supported by the SibratecNano-FINEP, FAPESP and CNPq-SisNano (Process 442497/2019-9) funding agencies.

Acknowledgments

The authors are grateful to the CCSNano-UNICAMP staff and Nacional de Grafite Ltda for support (providing expanded graphite samples) and an opportunity to conduct this research. This research used facilities of the Brazilian Nanotechnology National Laboratory (LNNano), part of the Brazilian Centre for Research in Energy and Materials (CNPEM), a private non-profit organization under the supervision of the Brazilian Ministry for Science, Technology, and Innovations (MCTI), proposal number: TEM-C1 - 25209.

Conflict of interest

The authors declare that the research was conducted in the absence of any commercial or financial relationships that could be construed as a potential conflict of interest.

Publisher's note

References

Alaferdov, A. V., Lebedev, O. V., Roggero, U. F. S., Hernandez-Figueroa, H. E., Nista, S. V. G., Trindade, G. M., et al. (2022). Highly conductive nanographite/ultra-high-molecular-weight polyethylene composite. *Results Mater* 15, 100298. doi:10.1016/j.rinma.2022.100298

Alaferdov, A. V., Savu, R., Canesqui, M. A., Kopelevich, Y. V., da Silva, R. R., Rozhkova, N. N., et al. (2018). Ripplocation in graphite nanoplatelets during sonication assisted liquid phase exfoliation. *Carbon* 129, 826–829. doi:10.1016/j.carbon.2017.12.100

Alaferdov, A. V., Savu, R., Fantini, C., Cançado, L. G., and Moshkalev, S. A. (2020). Raman spectra of multilayer graphene under high temperatures. *J. Phys. Condens. Matter* 32, 385704. doi:10.1088/1361-648X/ab95ce

Aturaliya, R., Wang, D., Xu, Y., Lin, Y., Li, Q., and Turng, L. (2020). Expanded polytetrafluoroethylene/graphite composites for easy water/oil separation. *ACS Appl. Mat. Interfac.* 12, 38241–38248. doi:10.1021/acsami.0c11583

Bernal, J. D. (1924). The structure of graphite. *Proc. R. Soc. Lond. Ser. A, Contain. Pap. Math. Phys. Character.* 106, 749–773.

Biniak, S., Szymański, G., Siedlewski, J., and Świątkowski, A. (1997). The characterization of activated carbons with oxygen and nitrogen surface groups. *Carbon* 35, 1799–1810. doi:10.1016/S0008-6223(97)00096-1

Bonnet, P., Sireude, D., Garnier, B., and Chauvet, O. (2007). Thermal properties and percolation in carbon nanotube-polymer composites. *Appl. Phys. Lett.* 91, 201910. doi:10.1063/1.2813625

Cançado, L. G., Jorio, A., Ferreira, E. H. M., Stavale, F., Achete, C. A., Capaz, R. B., et al. (2011). Quantifying defects in graphene via Raman spectroscopy at different excitation energies. *Nano Lett.* 11, 3190–3196. doi:10.1021/nl201432g

Cho, H., Kim, J., Park, S., Kim, S., Kim, H., Oh, H., et al. (2020). Demonstration of solar cell on a graphite sheet with carbon diffusion barrier evaluation. *Molecules* 25, 785. doi:10.3390/molecules25040785

Chung, D. D. L. (2016). A review of exfoliated graphite. *J. Mat. Sci.* 51, 554–568. doi:10.1007/s10853-015-9284-6

Danes, F., Garnier, B., and Dupuis, T. (2003). Predicting, measuring, and tailoring the transverse thermal conductivity of composites from polymer matrix and metal filler. *Inter. J. Thermophys.* 24, 771–784. doi:10.1023/A:1024096401779

Das, T. K., and Prusty, S. (2013). Graphene-based polymer composites and their applications. *Polym.-Plast. Technol. Eng.* 52, 319–331. doi:10.1080/03602559.2012.751410

Ding, J. N., Fan, Y., Zhao, C. X., Liu, Y. B., Yu, C. T., and Yuan, N. Y. (2012). Electrical conductivity of waterborne polyurethane/graphene composites prepared by solution mixing. *J. Compos. Mat.* 46, 747–752. doi:10.1177/0021998311413835

Dreyer, D. R., Murali, S., Zhu, Y., Ruoff, R. S., and Bielawski, C. W. (2011). Reduction of graphite oxide using alcohols. *J. Mat. Chem.* 21, 3443–3447. doi:10.1039/C0JM02704A

Forero-Sandoval, I. Y., Franco-Bacca, A. P., Cervantes-Álvarez, F., Gómez-Heredia, C. L., Ramírez-Rincón, J. A., Ordonez-Miranda, J., et al. (2022). Electrical and thermal percolation in two-phase materials: A perspective. *J. Appl. Phys.* 131, 230901. doi:10.1063/5.0091291

Frac, M., Pichór, W., and Szołdra, P. (2020). Cement composites with expanded graphite as resistance heating elements. *J. Compos. Mat.* 54, 3821–3831. doi:10.1177/0021998320921510

Fu, Y., Hansson, J., Liu, Y., Chen, S., Zehri, A., Samani, M. K., et al. (2019). Graphene related materials for thermal management. *2D Mater* 7, 012001. doi:10.1088/2053-1583/ab48d9

Fu, Y., Hou, M., Liang, D., Yan, X., Fu, Y., Shao, Z., et al. (2008). The electrical resistance of flexible graphite as flow field plate in proton exchange membrane fuel cells. *Carbon* 46, 19–23. doi:10.1016/j.carbon.2007.10.020

Ganguly, A., Sharma, S., Papakonstantinou, P., and Hamilton, J. (2011). Probing the thermal deoxygenation of graphene oxide using high-resolution *in situ* X-ray-based spectroscopies. *J. Phys. Chem. C* 115, 17009–17019. doi:10.1021/jp203741y

Han, W., Xiao, Y., Yin, J., Gong, Y., Tuo, X., and Cao, J. (2020). Fe3O4@Carbon nanofibers synthesized from cellulose acetate and application in lithium-ion battery. *Langmuir* 36, 11237–11244. doi:10.1021/acs.langmuir.0c01399

Hareesha, N., and Manjunatha, J. G. (2020). Fast and enhanced electrochemical sensing of dopamine at cost-effective poly (DL-phenylalanine) based graphite electrode. *J. Electroanal. Chem.* 878, 114533. doi:10.1016/j.jelechem.2020.114533

Hu, K., and Chung, D. D. L. (2011). Flexible graphite modified by carbon black paste for use as a thermal interface material. *Carbon* 49, 1075–1086. doi:10.1016/j.carbon.2010.10.058

Kondo, T., Ishiguro, J., and Watanabe, N. (1981). Process for producing flexible graphite product. *Pat. U. S.* 4, 244–934. Deposited: 13 jan.

Kundu, S., Wang, Y., Xia, W., and Muhler, M. (2008). Thermal stability and reducibility of oxygen-containing functional groups on multiwalled carbon nanotube surfaces: A quantitative high-resolution XPS and tpd/tpr study. *J. Phys. Chem. C* 112, 16869–16878. doi:10.1021/jp804413a

Kurian, A. S., Mohan, V. B., Souri, H., Leng, J., and Bhattacharyya, D. (2020). Multifunctional flexible and stretchable graphite-silicone rubber composites. *J. Mat. Res. Technol.* 9, 15621–15630. doi:10.1016/j.jmrt.2020.11.021

Lespade, P., Marchand, A., Couzi, M., and Cruege, F. (1984). Caracterisation de materiaux carbones par microspectrometrie Raman. *Carbon* 22, 375–385. doi:10.1016/0008-6223(84)90009-5

Li, B., Cao, X., Ong, H. G., Cheah, J. W., Zhou, X., Yin, Z., et al. (2010). All-carbon electronic devices fabricated by directly grown single-walled carbon nanotubes on reduced graphene oxide electrodes. *Adv. Mat.* 22, 3058–3061. doi:10.1002/adma.201000736

Li, B., and Zhong, W.-H. (2011). Review on polymer/graphite nanoplatelet nanocomposites. *J. Mat. Sci.* 46, 5595–5614. doi:10.1007/s10853-011-5572-y

Li, L., Wang, D., Chen, S., Zhang, Y., Wu, Y., Wang, N., et al. (2020). Effect of organic grafting expandable graphite on combustion behaviors and thermal stability of low-density polyethylene composites. *Polym. Compos.* 41, 719–728. doi:10.1002/pc.25401

Li, M., Gao, Ch., Hu, H., and Zhao, Zh. (2013). Electrical conductivity of thermally reduced graphene oxide/polymer composites with a segregated structure. *Carbon* 65, 371–373. doi:10.1016/j.carbon.2013.08.016

Li, M., Liu, J., Pan, S., Zhang, J., Liu, Y., Liu, J., et al. (2020). Highly oriented graphite aerogel fabricated by confined liquid-phase expansion for anisotropically thermally conductive epoxy composites. *ACS Appl. Mat. Interfac.* 12, 27476–27484. doi:10.1021/acsami.0c02151

López-Manchado, M. A., Herrero, B., and Arroyo, M. (2004). Organoclay-natural rubber nanocomposites synthesized by mechanical and solution mixing methods. *Polym. Int.* 53, 1766–1772. doi:10.1002/pi.1573

Luo, J., Yu, H., Wang, H., Wang, H., and Peng, F. (2014). Aerobic oxidation of benzyl alcohol to benzaldehyde catalyzed by carbon nanotubes without any promoter. *Chem. Eng. J.* 240, 434–442. doi:10.1016/j.cej.2013.11.093

Mindivan, F., and Göktaş, M. (2020). Preparation of new PVC composite using green reduced graphene oxide and its effects in thermal and mechanical properties. *Polym. Bull.* 77, 1929–1949. doi:10.1007/s00289-019-02831-x

Perrozzi, F., Prezioso, S., Donarelli, M., Bisti, F., De Marco, P., Santucci, S., et al. (2013). Use of optical contrast to estimate the degree of reduction of graphene oxide. *J. Phys. Chem. C* 117, 620–625. doi:10.1021/jp3069738

Pimenta, M. A., Dresselhaus, G., Dresselhaus, M. S., Cançado, L. G., Jorio, A., and Saito, R. (2007). Studying disorder in graphite-based systems by Raman spectroscopy. *Phys. Chem. Chem. Phys.* 9, 1276–1290. doi:10.1039/B613962K

Radouane, N., Maaroufi, A., Ouaki, B., Poupin, C., Cousin, R., Duponchel, B., et al. (2020). Thermal, electrical and structural characterization of zinc phosphate glass matrix loaded with different volume fractions of the graphite particles. *J. Non-Cryst. Solids* 536, 119989. doi:10.1016/j.jnoncrysol.2020.119989

Rashid, T., Sher, F., Hazafa, A., Hashmi, R. Q., Zafar, A., Rasheed, T., et al. (2021). Design and feasibility study of novel paraboloid graphite based microbial fuel cell for bioelectrogenesis and pharmaceutical wastewater treatment. *J. Environ. Chem. Eng.* 9, 104502. doi:10.1016/j.jece.2020.104502

Reiche, S., Blume, R., Zhao, X. C., Su, D., Kunkes, E., Behrens, M., et al. (2014). Reactivity of mesoporous carbon against water - an *in-situ* XPS study. *Carbon* 77, 175–183. doi:10.1016/j.carbon.2014.05.019

Ren, P. G., Yan, D. X., Ji, X., Chen, T., and Li, Z. M. (2011). Temperature dependence of graphene oxide reduced by hydrazine hydrate. *Nanotechnol* 22, 055705. doi:10.1088/0957-4484/22/5/055705

Sabzi, M., Jiang, L., Liu, F., Ghasemi, I., and Atai, M. (2013). Graphene nanoplatelets as poly(lactic acid) modifier: Linear rheological behavior and electrical conductivity. *J. Mat. Chem. A* 1, 8253–8261. doi:10.1039/c3ta11021d

Saglam, O., Dilgin, D. G., Ertek, B., and Dilgin, Y. (2016). Differential pulse voltammetric determination of eugenol at a pencil graphite electrode. *Mat. Sci. Eng. C* 60, 156–162. doi:10.1016/j.msec.2015.11.031

Sengupta, R., Bhattacharya, M., Bandyopadhyay, S., and Bhowmick, A. K. (2011). A review on the mechanical and electrical properties of graphite and modified graphite reinforced polymer composites. *Progr. Polym. Sci.* 36, 638–670. doi:10.1016/j.progpolymsci.2010.11.003

Shi, B., Dong, L., Li, M., Liu, B., Kim, K., Xu, X., et al. (2018). Thermal percolation in composite materials with electrically conductive fillers. *Appl. Phys. Lett.* 113, 041902. doi:10.1063/1.5039923

Sundar, J. V., and Subramanian, V. (2013). Novel chemistry for the selective oxidation of benzyl alcohol by graphene oxide and N doped graphene. *Org. Lett.* 15, 5920–5923. doi:10.1021/ol402958h

Teng, C., Xie, D., Wang, J., Yang, Z., Ren, G., and Zhu, Y. (2017). Ultrahigh conductive graphene paper based on ball-milling exfoliated graphene. *Adv. Funct. Mat.* 27, 1700240–1700247. doi:10.1002/adfm.201700240

Vanquickenborne, L. G., Vranckx, J., and Görller-walrand, C. (1974). Kinetic trans effect in square planar transition metal complexes. *J. Am. Chem. Soc.* 96, 4121–4125. doi:10.1021/ja00820a010

Vieira, F., Cisneros, I., Sansiviero, M. T. C., Miranda, A. M., Rosa, N. G., Lima, U. B., et al. (2006). Preparation processes and properties of expanded graphite for alkaline batteries. *J. Phys. Chem. Solids* 67, 1208–1212. doi:10.1016/j.jpcs.2006.01.050

Vithalani, R., Patel, D., Modi, C. K., Som, N. N., Jha, P. K., and Kane, S. R. (2018). Enhancing the potency of surface hydroxyl groups of graphene oxide for selective oxidation of benzyl alcohol. *Diam. Relat. Mat.* 90, 154–165. doi:10.1016/j.diamond.2018.10.015

Wang, P., Chong, H., Zhang, J., Yang, Y., and Lu, H. (2018). Ultralow electrical percolation in melt-compounded polymer composites based on chemically expanded graphite. *Compos. Sci. Technol.* 158, 147–155. doi:10.1016/j.compscitech.2018.01.022

Yamada, Y., Yasuda, H., Murota, K., Nakamura, M., Sodesawa, T., and Sato, S. (2013). Analysis of heat-treated graphite oxide by X-ray photoelectron spectroscopy. *J. Mat. Sci.* 48, 8171–8198. doi:10.1007/s10853-013-7630-0

Zanrosso, C. D., Piazza, D., and Lansarin, M. A. (2020). PVDF/ZnO composite films for photocatalysis: A comparative study of solution mixing and melt blending methods. *Polym. Eng. Sci.* 60, 1146–1157. doi:10.1002/pen.25368

Zhuang, Y., Zheng, K., Cao, X., Zhang, J., Ye, G., Ma, Y., et al. (2021). Graphene/naphthalene sulfonate composite films with high electrical and thermal conductivities for energy storage and thermal management in nanoscale electronic devices. *ACS Appl. Nano Mat.* 4, 13123–13131. doi:10.1021/acsanm.1c02643

Zotti, A., Zuppolini, S., Borriello, A., and Zarrelli, M. (2022). Polymer nanocomposites based on graphite nanoplatelets and amphiphilic graphene platelets. *Compos. Part B* 246, 110223. doi:10.1016/j.compositesb.2022.110223